

Full-Maxwell Simulations of Very Fast Transients in GIS: case study to compare 3D and 2D-axisymmetric models of 1100 kV test set-up

Marcin Szewczyk, *Senior Member, IEEE*, Kamil Kutorasiński,
Marcin Wroński, Marek Florkowski, *Senior Member, IEEE*

Abstract— Development- and type- testing of Gas-Insulated Switchgear (GIS) disconnectors are supported with simulation-based analyses of Very Fast Transients (VFT) that are associated with the disconnector switching operations. In order to analyze local field values in the entire GIS geometry, full-Maxwell approach needs to be involved for simulating of VFT generation process. According to power substation layout studies, 90°-angled GIS disconnectors are often used in GIS projects, as they offer most layout options and at the same time requiring lowest number of GIS components. This implies, that the test set-ups are asymmetric, thus direct use of the full-Maxwell approach requires 3D models, application of which is considered to be highly demanding from numerical point of view. The paper shows comparison of the results obtained from full-Maxwell numerical simulations for a development test set-up of 1100 kV GIS. The analyses are conducted for full 3D geometry and for the corresponding 2D-axisymmetric geometry. Example simulations of the VFT overvoltage (VFTO) waveforms are presented for both geometries, together with comparison of numerical effort needed for solving the associated field equations. The presented approach based on 2D-axisymmetric GIS model allows one to significantly reduce numerical effort involved to support design work and development tests.

Index Terms— Full-Maxwell wave analysis, Gas-Insulated Switchgear (GIS), Very Fast Transients (VFT)

I. INTRODUCTION

A. VFTO generation in GIS

VERY Fast Transient Overvoltages (VFTO) are generated in Gas-Insulated Switchgear (GIS) due to voltage breakdowns (flashovers) in SF₆ gas. They primarily occur during operations of the GIS disconnectors and as such cannot be avoided in any GIS substation. Due to physical properties

of the breakdown in SF₆ gas [1], typical rise time of the VFTO front (in the order of nanoseconds) is substantially smaller than the transit time of the associated electromagnetic wave through the GIS components. This causes that each of the voltage breakdowns generates travelling waves that propagate back and forth the GIS, being reflected and transmitted at any surge impedance discontinuity, and eventually being superimposed to constitute the VFTO in particular GIS component and at particular component's location.

B. VFTO numerical simulations

Simulation-based VFTO analyses are essential specifically for EHV and UHV class GIS [2]. For these high rated voltages, the insulation withstand voltage levels as defined in IEC Std. [3] are decreased as compared to the withstand voltage levels defined for lower rated voltages. This causes that for EHV and UHV class GIS the VFTO analyses are being extensively conducted to support design work and testing of the GIS components [4]. Moreover, VFTO studies are performed for power substations, being part of standard insulation co-ordination procedure, that is often ran at the stage of the substation planning [5].

Two approaches can in principle be applied for modeling of VFTO in GIS. Predominantly used approach is based on solving circuit equations for lumped and distributed equivalent circuit models, representing GIS components according to e.g. [6], [7]. The parameters of coaxial elements are calculated from standard formulas describing capacitance and inductance of coaxial-type conductors. Breakdown flashovers in SF₆ gas are represented by a non-linear resistance with the time constant defined by Toepler formula [8]. Operation of the disconnector is modelled with the disconnector design-specific Breakdown Voltage Characteristics [4]. The resulting overall equivalent model can be solved with the use of any transient simulation software based on solving circuit equations (e.g. EMTP-ATP [9]). The approach allows one to calculate voltage waveforms at the terminals of the GIS and/or substation components, as well as on the terminals of the substation adjacent power equipment, such as bushings and transformers [16]. However, direct application of the approach does not allow to calculate local field values for the GIS components of complex design, for which the relation between voltage

M. Szewczyk, M. Florkowski are with ABB Corporate Research Center, 31-038 Krakow, Starowiślna 13A, Poland (e-mail: marcin.szewczyk@pl.abb.com, marek.florkowski@pl.abb.com).

K. Kutorasiński is with ABB Transformer Technology Center, Łódź, Poland (e-mail: kamil.kutorasinski@pl.abb.com).

M. Wroński is with AGH University of Science and Technology, Faculty of Physics and Applied Computer Science, 30-059 Kraków, Mickiewiczza 30, Poland (email: marcin.wronski@fis.agh.edu.pl).

Corresponding author: M. Szewczyk (e-mail: marcin.szewczyk@pl.abb.com).

Color versions of one or more of the figures in this paper are available online at <http://ieeexplore.ieee.org>

(current) and electric (magnetic) field is unknown.

More general approach, yet numerically more demanding, is based on solving full-Maxwell equations for the actual GIS geometry and materials. This approach allows one to calculate the time-varying electromagnetic field distributions within the entire GIS. As such, the approach can serve for dielectric design of components to ensure that the electric field and its gradient spatial distributions are within limits that are acceptable for particular design of component.

C. State-of-the-art of full-Maxwell VFTO simulations

Only few papers have been published so far, addressing and/or utilizing VFTO modeling in GIS with the full-Maxwell approach. Reference [10] focuses on presenting feasibility of the full-Maxwell approach for modeling of VFTO in GIS. An example of time-domain simulations is shown in [10], conducted for a 3D GIS model, where Finite Element Method (FEM) is employed for solving field equations. Reference [11] presents calculation of resonance frequencies of a resonant cavity located in the GIS shielding elements. The analyses involve frequency-domain FEM simulations as opposed to more numerically demanding time-domain simulations presented in [10]. Reference [12] shows time-domain full-Maxwell FEM simulations, conducted for substantially simplified 2D-axisymmetric geometries, that are used in [12] with a purpose to illustrate a new design concept of the disconnecter contact system as introduced in [12]. The simulations shown in [12] does not involve complex details of real GIS design.

D. Paper context and structure

Fig. 1 shows an 1100 kV development test set-up with 90°-angled disconnecter used for analyses reported in the present paper. The design is asymmetric and thus for direct application of Maxwell simulations, the full 3D geometry is a natural choice. As shown in [10], solving full-Maxwell equations for a complex 3D GIS geometry model is very demanding from the calculation time and memory point of view. As an illustration of this statement, 15 hours have been quoted in [10] as a typical simulation time. This can largely limit applicability of the approach to solve problems that need many simulation runs, such as parametric/variation analyses for design optimization.

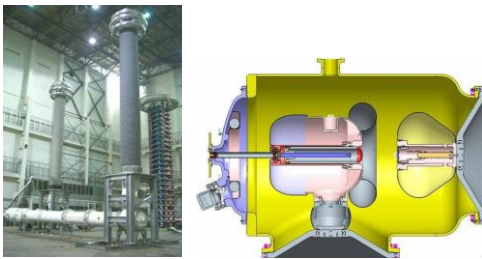


Fig. 1 Full scale test set-up according to IEC Std. [13] (left) with development design of 90°-angled 1100 kV GIS disconnecter (right) [4], [12].

In this paper, we present comparison between full-Maxwell simulations conducted for two geometries. First, we calculate VFTO for 3D geometry of 1100 kV GIS development test set-

up as shown in Fig. 1. Then we transform the 3D geometry into 2D-axisymmetric geometry and repeat VFTO simulations with the same test conditions employed. As a result, we show that the transformation from 3D (i.e. asymmetric) to 2D-axisymmetric GIS geometry does not sacrifice accuracy of VFTO simulations, while at the same time leads to substantial reduction of numerical effort. This shows applicability of the 2D-axisymmetric models for the GIS design work, that can be applied despite of the actual geometry asymmetry, and can lead to reduction of product development time and thus prototyping and type-testing cost.

This paper is organized as follows. Section I presents state-of-the-art methods that are in use for the VFTO simulations, giving context and aim of the work presented. In Section II, an 1100 kV test set-up is described, together with the simulation process used in the paper. The two geometry models of the test set-up are introduced: 3D and 2D-axisymmetric. Transformation of the 3D geometry model into 2D-axisymmetric model is shown. Section III presents example of VFTO simulation results obtained for the two geometries, together with computation effort associated with each of the simulation case. Section IV offers final conclusions.

II. SIMULATION PROCESS FOR 1100 kV TEST SET-UP

A. Test set-up according to IEC Standard

As the VFTO depends on particular design of the GIS disconnecter contact system, as well as on the project specific SF₆ gas pressure, standardization of VFTO waveform for testing is not feasible. Development- and type-tests of GIS disconnectors are thus conducted in the test set-ups where the VFTO is generated during operation of the disconnecter under test (see Fig. 1).

IEC Std. [13] defines test arrangement and testing procedure for VFTO generation for type testing of GIS disconnectors. This procedure is applicable for development tests as well. The worst case condition is defined for the disconnecter closing operation, when the disconnecter is operated with one of its side (the so called load side) pre-charged to a voltage of -1.1 p.u., while another side (the so called source side) is supplied from the AC 50/60 Hz voltage source of $+1.1$ p.u. (where $1 \text{ p.u.} = V_r \sqrt{2/3}$; V_r – rated voltage). The overall arrangement of the GIS components, jointly with the voltage settings, reflect highest possible VFTO conditions.

For VFTO simulations, both voltages defined in the test duty set-up (i.e. the pre-charged load side voltage and the amplitude of the alternating source side voltage) can be assumed as fixed. This is justified by the fact that the time duration of the VFTO process is significantly shorter than the AC 50/60 Hz alternation time and of the time constant of the DC voltage discharge. Moreover, the worst case breakdown condition most likely occur at the time instance when the AC 50/60 Hz voltage has its amplitude value.

B. Test set-up implementation in FEM simulation software

For simulations presented in this paper, the development

test set-up shown in Fig. 1 was modeled in COMSOL simulation software [14]. The VFTO generation process according to the IEC test procedure was employed as outlined above.

Fig. 2 shows part of the GIS geometry illustrating formulation of electromagnetic field equations as well as the boundary conditions employed. The field formulation was used as defined by magnetic vector potential $\vec{A}(\vec{r}, t)$ as a function of space coordinates \vec{r} and time of the testing process t :

$$\vec{\nabla} \times \mu_r^{-1}(\vec{\nabla} \times \vec{A}) + \mu_0 \sigma \frac{\partial \vec{A}}{\partial t} + \mu_0 \frac{\partial}{\partial t} \left(\epsilon_0 \epsilon_r \frac{\partial \vec{A}}{\partial t} \right) = 0, \quad (1)$$

where μ_0 is magnetic permeability of vacuum, μ_r is relative magnetic permeability, ϵ_0 is electric permittivity of vacuum, ϵ_r is relative electric permittivity, σ is conductivity. The magnetic potential $\vec{A}(\vec{r}, t)$ is used in (1) to represent the electric field $\vec{E} = -\frac{\partial \vec{A}}{\partial t}$ and the magnetic flux density $\vec{B} = \vec{\nabla} \times \vec{A}$ [15]. For the GIS components, $\mu_r = 1$ and $\epsilon_r = 1$ are used as representing properties of the SF₆ gas. For the time-domain simulations, zero initial condition of the magnetic potential was used: $\vec{A}(\vec{r}, 0) = 0$. All metal parts were represented by the boundary condition (BC) of Perfect Electric Conductor (PEC) type, that leads to zero tangential component of the electric field on the metal part surface:

$$\vec{n} \times \vec{E} = 0, \quad (2)$$

where \vec{n} is a vector normal to the metal part surface.

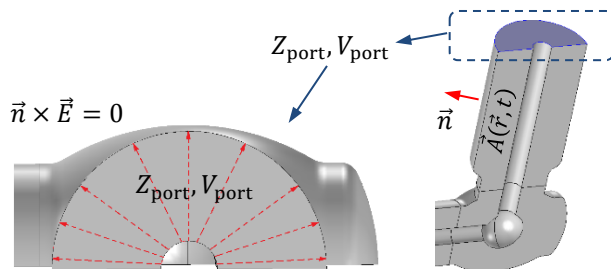


Fig. 2 Field formulation for calculation of magnetic potential $\vec{A}(\vec{r}, t)$ in (1); definition of Perfect Electric Conductor (PEC) boundary condition on metallic elements: $\vec{n} \times \vec{E} = 0$; definition of input voltage ports: $Z_{\text{port}}, V_{\text{port}}$.

The electromagnetic field computation domain consisted of the SF₆ gas region and the regions introduced for modeling of breakdown flashovers (see Section II.C below). Metal parts were not meshed and thus were excluded from the computation domain.

Voltage ports were characterized with input voltage and characteristic impedance, from which the magnetic potential $\vec{A}(\vec{r}, t)$ was calculated on port surfaces.

C. Model of voltage breakdown in GIS (spark)

Voltage breakdown in the GIS disconnector contact system (spark) was modeled as a cylindrical geometry bridging the

disconnecter contacts. The geometry was characterized by the conductivity σ , modeled as an exponential function of time t , with the time constant τ given by the Toepler formula [8] for SF₆ gas. The state-of-the-art exponential function proposed in [6], [7] for modeling the arc channel was modified to provide smooth transition from insulating to conducting state $\sigma_{i \rightarrow c}$ and from conducting to insulating state $\sigma_{c \rightarrow i}$, that ensures numerical stability of the time-domain simulations:

$$\begin{cases} \sigma_{i \rightarrow c}(t) = \sigma_0 \left[\frac{\exp\left(\frac{t-t_0}{\tau}\right)}{1 + \exp\left(\frac{t-t_0}{\tau}\right)} \right] \\ \sigma_{c \rightarrow i}(t) = \sigma_0 - \sigma_{i \rightarrow c}(t), \end{cases} \quad (3)$$

where σ_0 is conductivity in the steady conducting state, and t_0 is the time instance of the spark ignition for $\sigma_{i \rightarrow c}$, and of the spark extinction for $\sigma_{c \rightarrow i}$. According to this approach, the conduction of the spark is a sole function of time. The arc channel conductivity was changing in the whole spark region instantaneously according to the formula (3), and the spark geometry was cylindrical.

Fig. 3 shows time-dependent function of conductivity $\sigma_{i \rightarrow c}$ according to (3), for the spark ignition. Inset in Fig. 3 shows disconnector geometry with the voltage breakdown area indicated. The dimensions of the geometry, and the value of the steady state conductivity σ_0 , were selected so to provide the arc resistance of 0.5 Ω , as per e.g. [6].

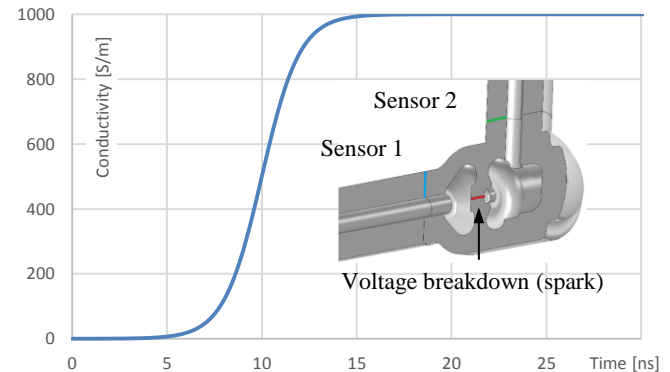


Fig. 3 Conductivity of voltage breakdown (spark) model for spark ignition $\sigma_{i \rightarrow c}$ according to (3); inset: disconnector geometry with breakdown voltage model indicated; integration lines in blue and green colors denote *Sensor 1* and *Sensor 2* respectively (in accordance with Fig. 4 and Fig. 5).

D. 3D and 2D-axisymmetric geometry models of test set-up

For the purpose of VFTO simulations presented in this paper, 3D geometry model of the test set-up shown in Fig. 1 was built. Fig. 4 shows the final geometry model consisting of the models of the following GIS components: disconnector under test (*DT*), auxiliary disconnector (*DA*), bus-bars, and elbows. *DA* was used to establish initial voltage conditions for VFTO generation in *DT* according to IEC Std. [13]. Voltage breakdown models are indicated in Fig. 4 within the contact system of each disconnector. The model is ended up with two ports (*Port 1* and *Port 2*) for defining voltage and characteristic impedance conditions at the test set-up ends.

The 3D model shown in Fig. 4 consists of two types of components with 90°-angled geometries: disconnectors and elbows. As these components pose no coaxial symmetry, they were transferred into the 2D-axisymmetric geometry, and this was done according to a procedure illustrated in Table I. The transformation was conducted under the condition that the lengths of the components over the lines indicated in Table I (a/b for elbow and ξ/ζ for disconnector) stay unchanged.

Table II shows capacitances of the elbow and the disconnector models calculated for both geometries (C_{3D} and C_{2D}). The capacitances were calculated from the volume integration of the electric energy density, stored in the model volume. It is shown in Table II, that only minor changes in the component's capacitances are introduced in the process of their geometry transformation (4.3% for elbows and 4.9% for disconnectors).

Fig. 5 shows the resultant 2D-axisymmetric geometry, as obtained from transformation (according to Table I) of the 3D geometry shown in Fig. 4.

TABLE I

TRANSFORMATION OF 3D GEOMETRY MODELS OF 90°-ANGLED COMPONENTS INTO 2D-AXISYMMETRIC GEOMETRY MODELS; A/B AND ξ/ζ DENOTE LENGTHS OF COMPONENTS ALONG THE LINES INDICATED; IMPLEMENTATION IN COMSOL SIMULATION SOFTWARE

	3D (see also Fig. 4)	2D (see also Fig. 5)
Elbow		
Disconnector		

TABLE II

CAPACITANCES OF ELBOW AND DISCONNECTOR COMPONENTS, CALCULATED FOR GEOMETRIES SHOWN IN TABLE I; $\delta = \frac{|C_{3D} - C_{2D}|}{C_{3D}} \cdot 100\%$

	C_{3D} (see also Fig. 4)	C_{2D} (see also Fig. 5)	δ
Elbow	47 pF	45 pF	4.3%
Disconnector	143 pF	136 pF	4.9%

E. Simulation sequence

The VFTO generation process was modeled according to the IEC procedure, as described in Section II.A. For the load side voltage, a voltage of -1.0 p.u. was used to reflect worst case scenario without safety margin.

In each simulation case, the simulation process consisted of two steps. In *Step 1*, the simulation started at the time instance

of $t = 0$ with the voltage at *Port 1* set at $t = 0$ to -1.0 p.u., and the voltage at *Port 2* set at $t = 0$ to $+1.1$ p.u. For any given time instance, the voltage at the port was a superposition of the voltage resulting from the initial condition and the voltage associated with a travelling wave coming to the port. Models of the voltage breakdowns occurring in the contact systems of *DT* and *DA* disconnectors, denoted as *Spark 1* and *Spark 2* respectively, were initially set to the conducting state (for *Spark 1*) and isolating state (for *Spark 2*). After relaxation to the steady state condition (at $t = 0.22 \mu\text{s}$, see Fig. 6), the conductivity of the *Spark 1* model was triggered to change its value from the conducting state to the insulating state. The conductivity in the process was given by (3). The bus-bar between *DA* and *DT* (see Fig. 4 and Fig. 5) was charged to the voltage value of -1.0 p.u., and the bus-bar between *DT* and *Port 2* was charged to the voltage value of $+1.1$ p.u. With these means, the voltage breakdown in *DA* model was used to establish initial voltage conditions for the VFTO generating process initiated later by the subsequent voltage breakdown in the *DT* model. In *Step 2* ($t = 0.22 \mu\text{s}$), the transition of *Spark 2* from insulated to conductive state was initiated according to Fig. 3 and (3). This second breakdown flashover initiated VFTO generation process.

For both models, as shown in Fig. 4 and Fig. 5, same voltage and boundary conditions, as well as same voltage breakdown model and sequence of operation, were employed.

III. SIMULATION RESULTS

A. VFTO simulated in 3D model

Fig. 6 shows results of time-domain VFTO simulations obtained in the 3D model shown in Fig. 4 according to the simulation process described in Section II. Voltage waveforms in Fig 6 are presented for two sensors, calculated as integrals of electric field along the lines indicated in Fig. 4 (denoted with blue color for *Sensor 1*, and green color for *Sensor 2*). *Step 1* and *Step 2* indicated in Fig. 6 reflect the simulation sequence as described in Section II.E. It can be seen from Fig. 6, that the VFTO generated in *Step 2* is constituted by multiple reflections from surge impedance discontinuities along the GIS. The peak of VFTO waveform in *Sensor 2* reaches 3.0 p.u. value.

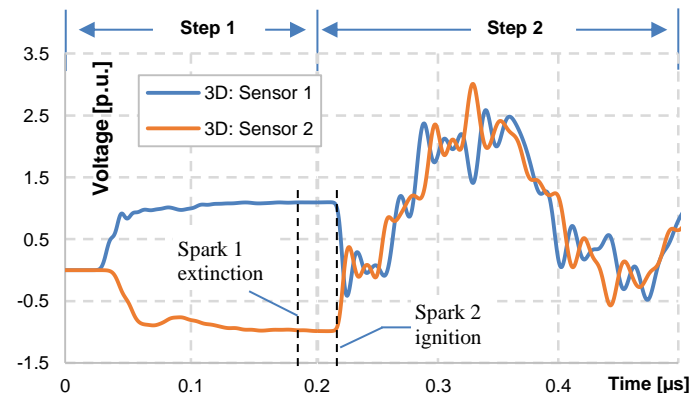


Fig. 6 VFTO waveforms simulated for 3D geometry model shown in Fig. 4, for two sensor locations (*Sensor 1* and *Sensor 2* according to Fig. 4);

simulation sequence involving two simulation steps (*Step 1* and *Step 2*) is described in Section II.E.

B. VFTO simulated in 2D-axisymmetric model

Fig. 7 and Fig. 8 show results of time-domain VFTO simulations in *Sensor 1* and *Sensor 2* respectively, obtained in *Step 2* of the same simulation process. The VFTO waveforms are obtained for the two geometry models: 3D and 2D-axisymmetric, as shown in Fig. 4 and Fig. 5 respectively. The voltage difference of the two waveforms is also shown in each figure. Results for 3D geometry in Fig. 7 and Fig. 8 are re-used from Fig. 6 (with same colors), for comparison purposes. In both geometry cases, all of the simulation conditions, the despite geometry, were used the same.

It can be seen in Fig. 7 and Fig. 8 that VFTO waveforms calculated for both geometry models are in good agreement. From Fig. 7, the VFTO waveforms difference, for VFTO peak value for *Sensor 2*, can be read as 0.15 p.u., which is 5.1% of the VFTO peak value of *Sensor 2* for 3D geometry.

Fig. 5 depicts example of spatial distribution of electric field norm during the VFTO generation process, at the time instance of $t = 0.33 \mu\text{s}$ when the VFTO waveform shown in Fig. 7 (*Sensor 2*) reaches its peak value.

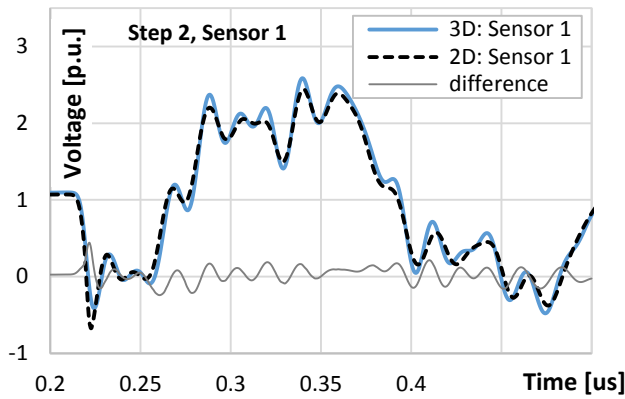


Fig. 7 Comparison of VFTO waveforms simulated for 3D and 2D axisymmetric geometry models (according to Fig. 4 and Fig. 5 respectively), with the waveforms difference, for *Sensor 1* location (according to Fig. 4 and Fig. 5); for *Step 2* of simulation sequence as shown in Fig. 6 and described in Section II.E; grey line indicates voltage difference.

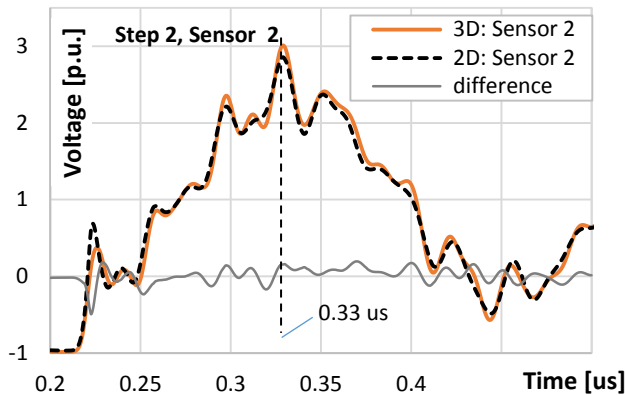


Fig. 8 Comparison of VFTO waveforms simulated for 3D and 2D axisymmetric geometry models (according to Fig. 4 and Fig. 5 respectively), with the waveforms difference, for *Sensor 2* location (according to Fig. 4 and Fig. 5); for *Step 2* of simulation sequence as shown in Fig. 6 and described in

Section II.E; spatial distribution of electric field norm for $t = 0.33 \mu\text{s}$ shown in Fig. 5.

C. Comparison of numerical effort

Table III shows comparison of numerical effort N_{eff} for VFTO simulations with 3D model (shown in Fig. 4) and with 2D-axisymmetric model (shown in Fig. 5). The comparison was performed for similar spatial-temporal resolution used for both models. Among other parameters, substantial reduction of computation time was observed (by factor $k = 45.3$).

IV. CONCLUSIONS

Earlier research has shown [10], that full-Maxwell simulations of Very Fast Transients (VFT) in Gas-Insulated Switchgear (GIS), conducted for 3D geometry model, are in principle feasible, however require high numerical effort and thus long computation time. Typical GIS layouts, as well as the designs of some GIS components, are asymmetric, therefore for direct application of Maxwell simulations the 3D geometry is a natural choice.

TABLE III

COMPARISON OF NUMERICAL EFFORT N_{eff} FOR VFTO SIMULATIONS SHOWN IN FIG. 6 AND FIG. 7, OBTAINED FOR 3D GEOMETRY MODEL SHOWN IN FIG. 4 AND FOR 2D-AXISYMMETRIC MODEL SHOWN IN FIG. 5; $k = NE_{3D}/NE_{2D}$

	N_{eff}^{3D} (see Fig. 4)	N_{eff}^{2D} (see Fig. 5)	k
Mesh elements			
Domain elements	50 087	3 561	14.1
Boundary elements	12 218	632	19.3
Edge elements	1 538	n/a	n/a
Degrees of freedom	345 262	26 078	13.2
Solver settings			
Time range	0 – 1.5 μs		n/a
Time step	1 ns (fixed)		n/a
Physical memory	5.26 GB	2.34 GB	2.3
Virtual memory	5.79 GB	2.50 GB	2.3
Solution time	2 hours 13 minutes 43 seconds	0 hours 2 minutes 57 seconds	45.3

In this paper, an 1100 kV development test set-up was used to present feasibility of the full-Maxwell VFT simulations in 2D-axisymmetric geometry. Transformation of the test set-up asymmetric 3D geometry to 2D-axisymmetric geometry model was presented. The VFT overvoltage (VFTO) waveforms obtained from full-Maxwell simulations for both models, 3D and 2D-axisymmetric, were compared. The waveforms are in good agreement, showing that modeling of the GIS with 2D-axisymmetric model is feasible and gives

accurate results as compare to the 3D model. Significant reduction of numerical effort was achieved. The computation time needed for VFTO simulation was shown to be reduced by factor 45.

The work here presented may result in increased use the full-Maxwell approach for simulations supporting research and technology development related with GIS. As indicated in the paper, publications using this approach are rare up to the moment, as compared to the alternative approach based on solving circuit equations.

REFERENCES

- [1] G. Ecklin and D. Schlicht, "Overvoltages in GIS caused by the operation of isolators," in *Proc. 1979 of the Brown Boveri Research Centre*, Baden, Switzerland, September 3-4, 1979.
- [2] U. Riechert and W. Halaus, "Ultra high-voltage gas-insulated switchgear – a technology milestone," *European Transactions on Electrical Power*, vol. 22, no. 1, pp. 60–82, May 2011.
- [3] *High-Voltage Switchgear and Controlgear – Part 203: Gas-Insulated Metal-enclosed Switchgear for Rated Voltages Above 52 kV*, IEC Standard 62271-203, Nov. 2003.
- [4] M. Szewczyk, M. Kuniewski, W. Piasecki, M. Florkowski, and U. Straumann, "Determination of Breakdown Voltage Characteristics of 1100 kV disconnecter for modeling of VFTO in Gas-Insulated Switchgear," [submitted for publication in *IEEE Trans. Power Delivery*]
- [5] CIGRE Working Group C4.306, "Insulation Coordination for UHV AC Systems," *CIGRE Technical Brochure 542*.
- [6] D. Povh, H. Schmitt, O. Volcker, R. Witzmann, P. Chewdhuri, A. E. Imece, R. Irvani, J. A. Martinez, A. Keri, and A. Sarshar, "Modeling and Analysis Guidelines for Very Fast Transients," *IEEE Power Engineering Review*, vol. 17, no. 13, 1996.
- [7] J. A. Martinez, D. Povh, P. Chowdhuri, R. Irvani, and A. J. F. Keri, "Modeling Guidelines for Very Fast Transients in Gas Insulated Substations," *IEEE PES Special Publication of the IEEE Working Group on Modeling and Analysis of System Transients*, 1998.
- [8] S. A. Boggs, F. Y. Chu, N. Fujimoto, A. Krenicky, A. Plessl, and D. Schlicht, "Disconnect Switch Induced Transients and Trapped Charge in Gas-Insulated Substations," *IEEE Trans. Power Apparatus and Systems*, vol. PAS-101, No. 10, 1982.
- [9] H. W. Dommel, W. S. Meyer: "Computation of electromagnetic transients," *Proceedings of the IEEE*, vol. 62, no. 7, July 1974, pp. 983-993.
- [10] J. Smajic, W. Halaus, J. Kostovic, and U. Riechert, "3D Full-Maxwell Simulations of Very Fast Transients in GIS," *IEEE Trans. Magnetics*, vol. 47, No. 5, pp. 1514-1517, May 2011.
- [11] J. Smajic, A. Shoory, S. Burow, W. Halaus, U. Riechert, and S. Tenbohlen, "Simulation-Based Design of HF Resonators for Damping Very Fast Transients in GIS," *IEEE Trans. Power Delivery*, vol. 29, No. 6, pp. 2528-2533, Dec 2014.
- [12] M. Szewczyk, W. Piasecki, M. Wroński, and K. Kutorasiński, "New Concept for VFTO Attenuation in GIS with Modified Disconnecter Contact System," *IEEE Trans. Power Delivery*, vol. 30, No. 5, pp. 2138-2145, Dec 2014.
- [13] *High-Voltage Switchgear and Controlgear—Part 102: Alternating Current Disconnectors and Earthing Switches*, IEC 62271-102.
- [14] COMSOL Multiphysics. [Online]. Available: www.comsol.com
- [15] D. J. Griffiths, "Introduction to Electrodynamics", 3rd edition, *Prentice Hall*, 1999.
- [16] CIGRE JWG A2-A3-B3.21, "Electrical Environment of Transformers – Impact of Fast Transients", *Electra* No. 218, Feb. 2005, pp. 25-37.



Marcin Szewczyk (M'2012–SM'2014) received his M.Sc. and Ph.D. degrees in Electrical Engineering from Warsaw University of Technology, Warsaw, Poland, in 2000 and 2009 respectively. He was Assistant Professor at Warsaw University of Technology. Since 2010 he is a Researcher with ABB Corporate Research in Cracow, Poland. His research is mainly in the field of power system analyses and advanced simulations, power products, transients analyses and transients mitigation, insulation coordination, 3D modeling and simulations of electromagnetic fields, modeling of magnetic materials for transient analyses, modeling of Vacuum Circuit Breakers.

Dr. Szewczyk is a member of IEEE and Polish Society for Theoretical and Applied Electrical Engineering (ABB Corporate Research, Starowiślna 13A, 31-038 Krakow, Poland, E-mail: marcin.szewczyk@pl.abb.com).



Kamil Kutorasiński (1985), received his M.Sc and Ph.D. in physics from the University of Science and Technology in Kraków. His research was in the field of transport properties in advanced material based on ab initio DFT methods as well as FEM modelling and simulations of electromagnetic fields. Since 2015 he works with ABB Transformer Technology Center in Poland (E-mail: kamil.kutorasinski@pl.abb.com).



Marcin Wroński (1984), received M.Sc. degree in Physic from the AGH University of Science and Technology (UST) Kraków, Poland, in 2009. In the same year he started PhD studies parallel at the AGH UST and University Paris 13 in the co-tutelle system. He obtained double PhD degree in Physics and Mechanics of Materials, in 2013 (graduated with honors). He is currently working as a research assistant at AGH University of Science and Technology Kraków. His research interests are in the field of material science: development of

polycrystalline deformation models, experimental work using EBSD and X-Ray diffraction technique. His research include modelling of electromagnetic fields using FEM.



Marek Florkowski (M'97-SM'08) received the M.S. and Ph.D. degrees in electronics from AGH University of Science and Technology in Kraków in 1990 and 1994, respectively. From 1990 to 1992 he was employed at ABB Corporate Research Center in Baden-Dättwil. In 2009 he obtained habilitation. He is currently responsible for ABB Corporate Research in Krakow, Poland. A member of CIGRE, and APEE. He is chair of the Technical Committee on Diagnostics of the IEEE Dielectrics and Electrical Insulation Society.

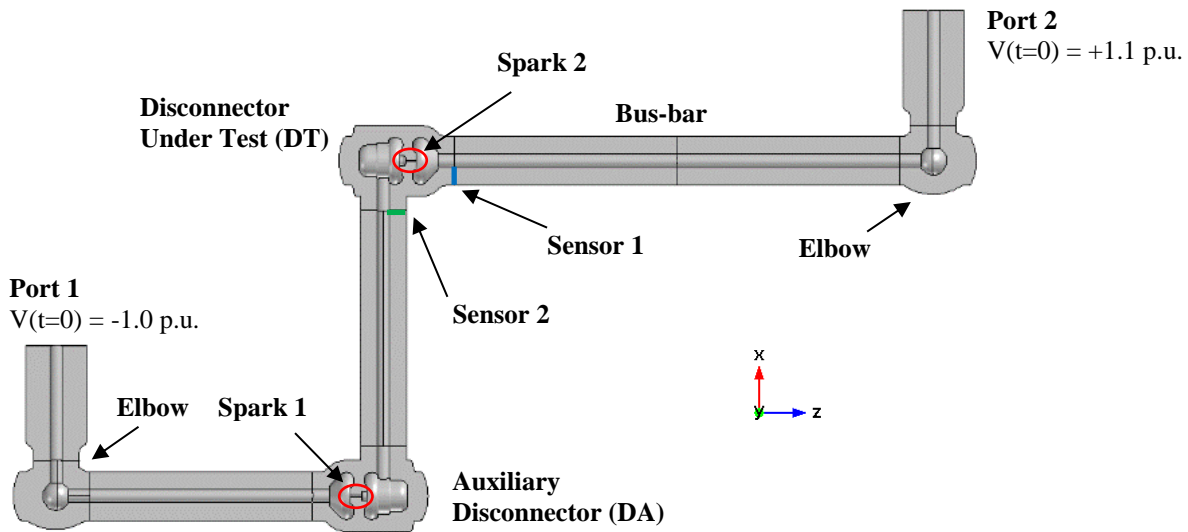


Fig. 4 3D geometry model of full scale 1100 kV test setup shown in Fig. 1; integration lines in blue and green colors denote *Sensor 1* and *Sensor 2* respectively (see also Fig. 5); test set-up used for simulation of VFTO as shown in Fig. 6 and Fig. 7; implemented in COMSOL simulation software.

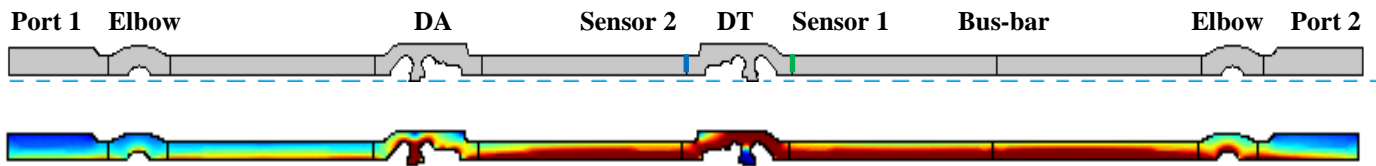


Fig. 5 2D-axisymmetric geometry model of the full scale 1100 kV test setup shown in Fig. 1; obtained by transformation of 3D geometry model shown in Fig. 4 according to the procedure illustrated in Table I; integration lines in blue and green colors denote *Sensor 1* and *Sensor 2* respectively (see also Fig. 4); test set-up used for simulation of VFTO as shown in Fig. 7; bottom figure shows example of spatial distribution of electric field norm during VFTO generation process, at the time instance of $t = 0.33 \mu\text{s}$ when the VFTO waveform shown in Fig. 8 reaches its peak value at *Sensor 2*; implemented in COMSOL simulation software.

